PHYSOR 2004 -The Physics of Fuel Cycles and Advanced Nuclear Systems: Global Developments
Chicago, Illinois, April 25-29, 2004, on CD-ROM, American Nuclear Society, Lagrange Park, IL. (2004)

Passive Decay Heat Removal in a Fluidized Bed Nuclear Reactor

A. Agung[1], D. Lathouwers[1*], T.H.J.J. van der Hagen[1], H. van Dam[1]
C.C. Pain[2], C.R.E. de Oliveira[3], A.J.H. Goddard[2], M.D. Eaton[2], J.L.M.A. Gomes[2], B. Miles[2]

[1]Interfaculty Reactor Institute, Delft University of Technology,
Mekelweg 15, 2629 JB Delft, The Netherlands
[2]Department of Earth Science and Engineering,
Imperial College of Science, Technology and Medicine, London SW7 2BP, United Kingdom
[3]Nuclear & Radiological Engineering and Medical Physics Program,
The George W. Woodruff School of Mechanical Engineering, Georgia Institute of Technology,
Atlanta, GA 30332-0405, USA

Numerical simulations have been performed to investigate the possibility of passive decay heat removal in a fluidized bed nuclear reactor. The conduction, convection and radiative heat transfer were included and the high Reynolds number k-ε turbulence model was applied for the flow calculations. A P_1 approximation method for participating media was used for the radiation model. The reactor was modeled as a 2D axisymmetric cylinder. Calculations were performed for different initial total operating power to see whether the associated decay heat can be removed by passive means without compromising the safety margin. The results show the decay heat can be removed by passive means up to operating powers of about 55 MW. Further the results showed that all heat transfer mechanisms are of importance to remove heat from the bed of fuel particles to the reflector.

KEYWORDS: decay heat, fluidized bed nuclear reactor, passive heat removal, numerical simulation.

1. Introduction

The Fluidized Bed Thermal Fission Nuclear Reactor (FLUBER) is an innovative reactor design utilizing the concept of gas-solid fluidization. It consists of TRISO coated fuel particles contained in a graphite-walled cylinder. Helium is used as a coolant and as fluidizing medium. When there is no flow of helium into the core or when the upward flow is small enough, the fuel particles are packed at the bottom of the core and the reactor is strongly subcritical as a result of a lack of moderation. As the flow increases, the particles are fluidized, the core expands and the reactivity increases due to increasing moderation by the graphite reflectors.

The design was recently modified to allow for a larger shutdown margin and higher output power [1, 2]. General specifications of the current FLUBER design are listed in Table 1 and Figure 1 shows the schematic view of the reactor at packed bed and fluidized conditions.

[*] Corresponding author, Tel. +31 15 2783148, Fax. +31 15 2786422, email: d.lathouwers@iri.tudelft.nl

Table 1. FLUBER specifications

Radius of the core cavity [cm]	79.8
Height of the core cavity [cm]	600
Height of the whole reactor [cm]	800
Thickness of the axial and radial reflector [cm]	100
Thickness and height of radial absorber [cm]	50
Concentration of radial absorber [ppm]	50
Collapsed-bed height (at 40% of porosity) [cm]	122.36
Uranium inventory [kg]	220
Enrichment [% weight]	16.76
Helium pressure [bar]	60
Maximum power (at full expansion) [MW]	120
Maximum fuel temperature [K]	1165
Maximum gas temperature [K]	1160

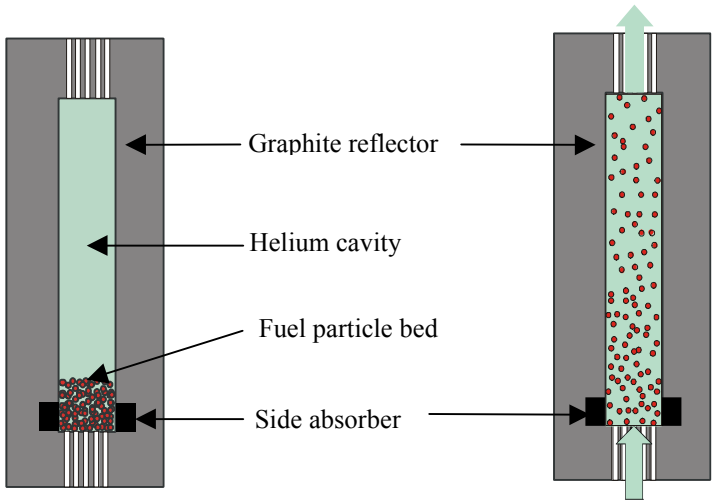

Fig. 1 A schematic view of FLUBER at packed state (left) and fluidized state (right). The size of the fuel particles is not to scale.

When the flow of helium through the core is reduced either intentionally or by pump failure, the bed of fuel particles forms a packed state. However, decay heat is still produced and has to be removed safely. In the worst-case scenario where no pump is available, heat has to be removed by passive means. As the initial total output power is relatively high, the decay heat removal after reactor shutdown becomes of major importance. In the case of operation at full bed expansion, for instance, the maximum total power can reach 120 MW with a maximum fuel temperature of 1165 K and after shutting down the reactor (by not introducing helium into the reactor), the bed becomes packed at about 2.5 m^3 of core volume. Initially the decay power is about 7% of the total power, giving a decay power density of around 3.4 MW/m^3.

The objective of this research is to investigate whether the associated decay heat can be removed by passive means without compromising the safety criterion. For coated fuel particles, IAEA recommends the value of 1873 K as a conservative limit on peak fuel temperature under accident conditions [3].

2. Mathematical Model

The decay heat removal in FLUBER can be described by combining heat transfer in a porous medium, conduction, convection and radiation. The incident scenario considered is that the system remains at the operating pressure of 60 bar and that the system has no forced convection through it. The system is modeled as being closed which is at odds with the assumption of constant pressure. Therefore, a stationary mass balance is enforced rather than the complete mass conservation equation. This assumption is valid as the flow field is quasi stationary on the timescales considered.

2.1. Flow model

2.1.1.Continuity equation

The continuity equation for the gas phase is

$$\nabla \cdot \left(\alpha_g \rho_g \mathbf{u} \right) = 0 \tag{1}$$

where α is the volume fraction, ρ is the density, $\mathbf{u}$ is the velocity vector and the index g represents the gas phase.

2.1.2. Momentum equation

The momentum equation for the gas phase can be written as [4,5]:

$$\frac{\partial \left(\alpha_g \rho_g \mathbf{u} \right)}{\partial t} + \nabla \cdot \left(\alpha_g \rho_g \mathbf{u}\mathbf{u} \right) = -\frac{\alpha_p \rho_p}{\tau_{12}} \mathbf{u} + \nabla \cdot \alpha_g \bar{\bar{\tau}}_g - \alpha_g \nabla P + \alpha_g \rho_g g \tag{2}$$

where τ_{12} is the gas-particle interaction time scale calculated from the classical Ergun relation, $\bar{\bar{\tau}}$ is the stress tensor, P is pressure, the index p represents the solid phase and g is the gravitational acceleration. The gas is further assumed to obey the ideal gas law.

For solving the flow calculations, the high Reynolds k-ε turbulent model is applied.

2.1.3. Energy equation

The gas phase and solid phase energy equations are

$$\alpha_g \rho_g C_{p,g} \frac{D_g T_g}{Dt} = \nabla \cdot \left[\alpha_g \lambda_g \nabla T_g \right] + h_{pg} a_{pg} \left[T_p - T_g \right] \tag{3}$$

$$\alpha_p \rho_p C_{p,p} \frac{\partial_p T_p}{\partial t} = \nabla \cdot \left[\alpha_p \lambda_p \nabla T_p \right] - h_{pg} a_{pg} \left[T_p - T_g \right] + P_d''' - S_{rad} \tag{4}$$

$$\rho_{refl} C_{p,refl} \frac{\partial T_{refl}}{\partial t} = \nabla \cdot \left[\lambda_{refl} \nabla T_{refl} \right] \tag{5}$$

where C_p is the heat capacity, T is the temperature, λ is the thermal conductivity, h_{pg} is the heat transfer coefficient between gas and solid phase obtained from the standard Ranz correlation, a_{pg} is the interfacial area per unit volume of the solid particles, P_d''' is the volumetric decay heat source, S_{rad} is the radiation heat source and the index *refl* represents the reflector part. Properties of the gas and solid phase are obtained from available data [6-8].

2.2. Radiation model

The radiation heat transfer is modeled using the integro-differential equation for participating media [9],

$$\mathbf{\Omega}\cdot\nabla I+\Sigma_t I=\Sigma_a I_b+\frac{\Sigma_s}{4\pi}\int_{4\pi} I\left(\mathbf{\Omega}'\right)\Phi\left(\mathbf{\Omega}'\cdot\mathbf{\Omega}\right)d\Omega' \tag{6}$$

where I is the intensity of radiation, I_b is the black-body intensity ($\sigma T^4/\pi$), Σ_t is the extinction coefficient, Σ_s is the scattering coefficient, Σ_a is the absorption coefficient, σ is the Stefan-Boltzman constant, $\mathbf{\Omega}$ is the direction vector and Φ is the scattering phase function, describing the probability that a ray from direction $\mathbf{\Omega}'$ will be scattered into a certain direction $\mathbf{\Omega}$. In our calculation isotropic scattering is assumed.

The radiative properties of the particles are obtained from the independent theory, meaning that the absorption and scattering characteristics of a particle is not influenced by its neighboring particles. Further for large spheres compared to the thermal wavelength the following relations apply

$$\Sigma_a=\Sigma_s=\frac{3}{2}\frac{\alpha_p}{d_p} \tag{7}$$

$$\Sigma_t=3\frac{\alpha_p}{d_p} \tag{8}$$

where d_p is the particle diameter. Helium in the cavity is transparent to thermal radiation, hence does not participate in the radiative processes.

The radiation model is solved using the P_1 approximation, leading to a diffusion equation as

$$D\nabla\cdot\nabla\varphi+\Sigma_a\varphi=\Sigma_a I_b \tag{9}$$

where D is the diffusion coefficient ($=-1/3\Sigma_t$), and φ is the scalar radiation intensity.

The radiative transfer (Eq. 6) is then coupled to the energy equation (Eq. 4) through the radiation source,

$$S_{rad}=\Sigma_a\left[4\sigma T_p^4-\int_{4\pi} I\left(\mathbf{\Omega}\right)d\Omega\right] \tag{10}$$

2.3. Decay power

The reactor is assumed to be operated long enough before shutdown so that the decay power has achieved steady state. The decay power, P_d, after shutdown can then be expressed in the following form:

$$P_d=\frac{P_{tot}}{Q_f+\sum_{n=1}^{N_d}\frac{\gamma_n}{\lambda_n}}\sum_{n=1}^{N_d}\frac{\gamma_n}{\lambda_n}e^{-\lambda_n t} \tag{11}$$

where P_{tot} is the total generated power before shutdown, Q_f is the prompt recoverable energy per fission, γ_n and λ_n are the decay heat yield and the decay heat constant, respectively and N_d is number of decay heat groups (for our purpose, we use 23 groups) [10]. Figure 2 (left) shows the percentage of decay heat of the total power during a 12 hour period after shutdown.

The volumetric heat source in Eq. 6 is given as

$$P_d''' = P_d / V_{core} \tag{12}$$

where V_{core} is the core volume. Note that the decay heat source is generated homogeneously in the packed bed as a result of the homogeneous burn-up of fuel during the fluidization process owing to the excellent mixing associated with fluidization.

2.4. Initial and boundary conditions

The initial temperature of particles and helium is uniform through the bed and the cavity in accordance with the good mixing mentioned earlier. The initial values of the temperatures are obtained from preceding calculations using a point dynamics code and are listed in Table 2. The initial values of reflector temperature is obtained from a steady-state 2D calculation with the outer wall boundary is set to 298 K and the inner wall boundary is set to 800K. The initial velocity of the gas is set to zero.

The boundary condition for the temperature at the side and top outer walls is obtained from the natural convective and gray body radiation to the atmosphere while the temperature of the bottom reflector wall is assumed constant at 500 K. The atmospheric temperature in this case is 298 K.

At the internal boundary between the reflector and core, the boundary conditions are obtained from the three heat transfer modes. With regard to the incoming radiation flux into the reflector, the wall is assumed to be a diffusely emitting and reflecting opaque surface. In terms of convective-conductive mode, the boundary conditions are obtained from the turbulence wall functions for gas velocities and gas temperature.

The fuel volume fraction is constant at 0.6 in the bed and 10^{-3} in the cavity for the reason that will be explained in a later section.

Table 2. Initial values of parameters

Total Power (MW)	Fuel temperature (K)	Gas Temperature (K)
30	761	760
40	821	820
50	875	874
60	922	920
70	967	966

3. Solution Methodology

The set of partial differential equations was solved using a finite volume method with a staggered grid for a two-dimensional axisymmetric cylinder. All convective fluxes are approximated with a second-order bounded TVD scheme. The time discretization is based on a backward Euler scheme in combination with a pressure-correction technique.

All sparse linear systems arising from the discretization of convection-diffusion systems are solved with conjugate gradient (CG) for the pressure equation and Generalized Minimum RESidual (GMRES) for the other transport equations. Preconditioning of these linear solvers was based on ILU factorization.

4. Results

The geometry of the reactor was discretized in a 2D axisymmetric cylindrical coordinate with an inhomogeneous mesh. The core is discretized into 20 (radial) by 120 (axial), while the height of the packed bed is discretized into 26 control volumes. The reflectors are meshed with 20 additional control volumes in radial and axial directions.

All calculations were performed with a time step of 0.25 seconds, with the capability to save the results and restart the problem every 900 seconds of real time. The simulations were run for 12 hours of real time. Such calculations demand approximately 12 hours of CPU time, running on an AMD Athlon XP1800+.

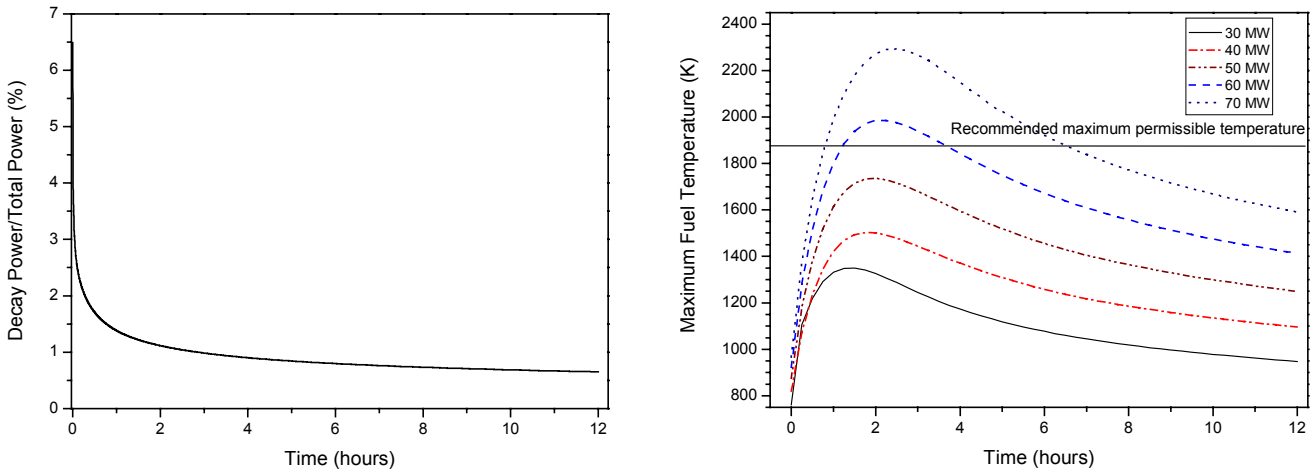

Fig. 2 Percentage of decay power to the initial total power after shutdown of the reactor (left), the time evolution of the maximum fuel temperature for different initial operating power (right).

The time evolution of the maximum fuel temperature for different initial total power is shown in Figure 2 (right). The thermal transient in the active core shows an increase of the fuel temperature over the first few hours to reach peak temperature followed by a gradual cool down. The core initially heats up slowly as the decay heat generation exceeds the heat removal rate. Later the active core heat removal rate exceeds the decay heat generation rate and from then on the average core temperature decreases slowly as heat is transferred to the reflector and atmosphere.

The maximum fuel temperature for high initial total power reaches its peak at later time. Inside the core, the dominant heat transfer mechanism on short time-scales is conduction. The conductivity of the solid phase is in fact a function of temperature and its value decreases quite significantly at higher temperatures. Hence at higher heat production rate, the solid phase becomes less efficient in transferring energy.

Figure 2 also shows clearly that at an operating power of 60 MW the peak fuel temperature exceeds the recommended maximum permissible temperature.

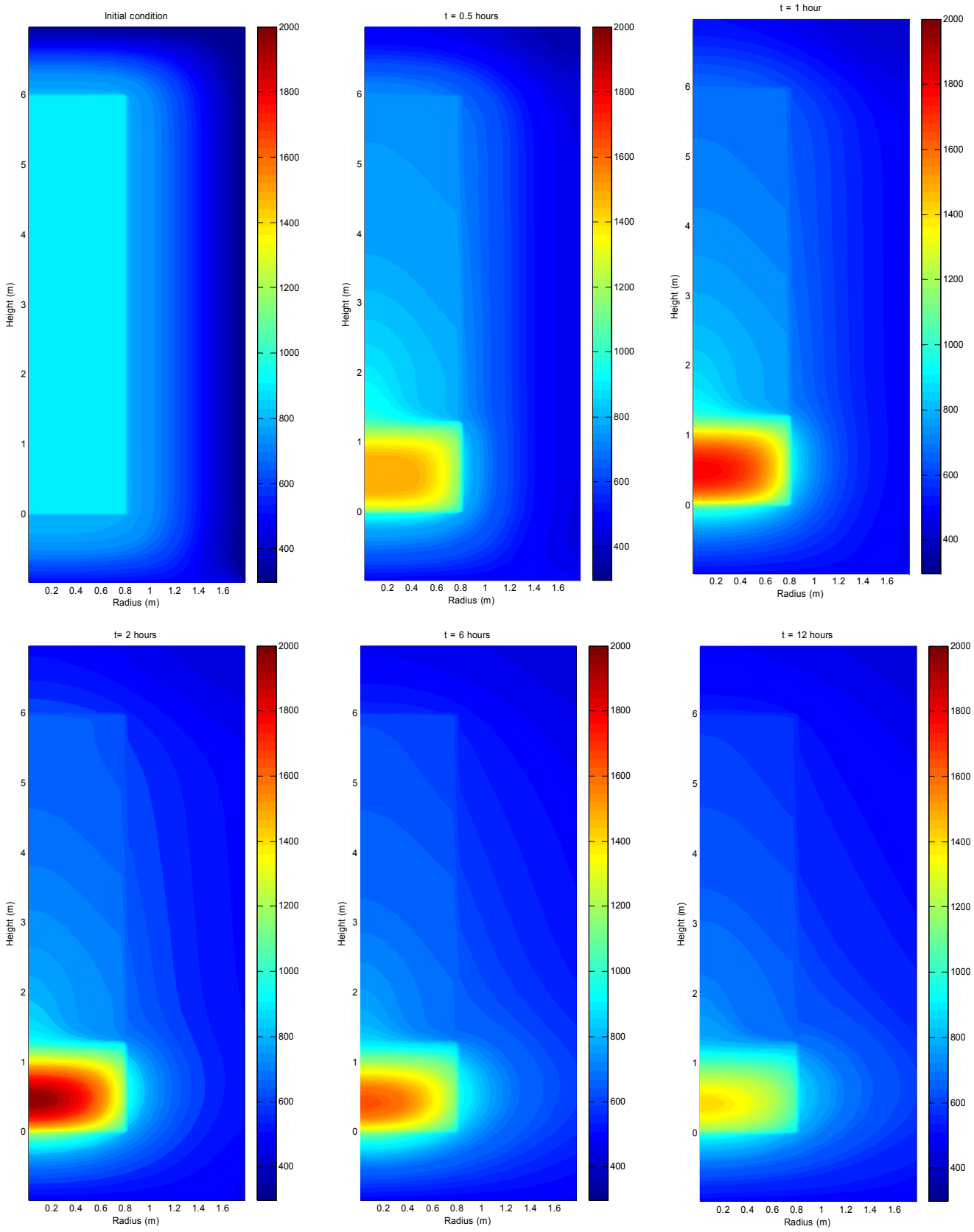

Fig. 3 The fuel temperature in the bed, the helium gas temperature in the cavity and the graphite temperature in the reflector at different times after shutdown at initial operating power of 60 MW.

Figure 3 visualizes the combined temperature fields (i.e. fuel temperature in the bed, gas temperature in the cavity and graphite temperature in the reflector) for an initial operating power of 60 MW. Initially, the fuel and helium temperature are uniform as a result of well-mixed of particles during the previous fluidization process. Up to 2 hours after shutdown, the core heats up as the decay heat is still dominant. It can be seen as well that at the top of the particle bed the temperature gradient is quite large caused by the flow of colder helium running over it. Large temperature gradients also can be seen in the interface of bed and the bottom/side reflector and in this case the presence of conductive/radiative transfer is the main cause. After the peak temperature is reached at about 2 hours after shutdown, the core experiences a slow cooling down.

Figure 4 (left) shows the helium flow field inside the reactor at 2 hours after shutdown for an initial operating power of 60 MW. Note that some mesh points are omitted in this graph for clarity reason. The flow field develops quickly and the transient behaves in a quasi-static manner at later time. The flow inside the packed region is virtually absent owing to the high associated pressure drop in this region and the heat transfer from the particles toward the gas is strictly diffusional.

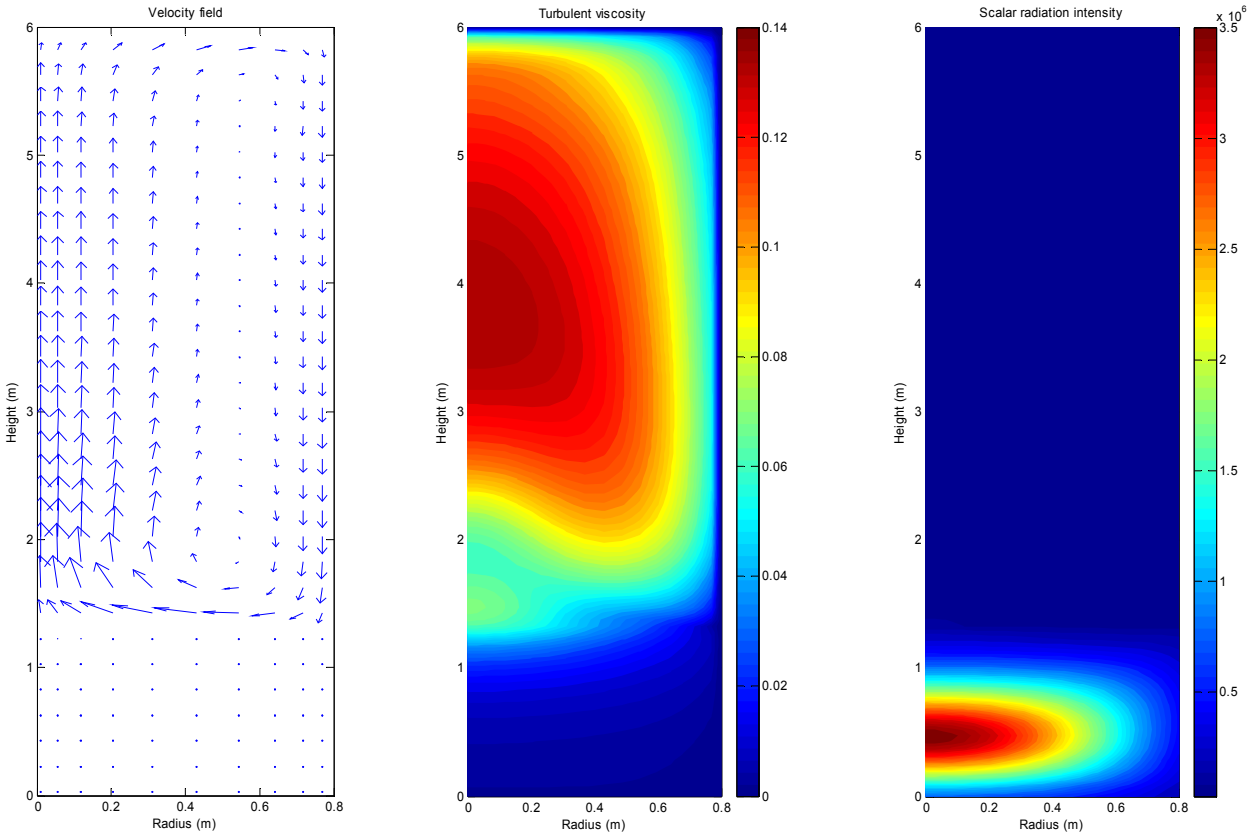

Fig. 4 The flow field of helium (left), turbulent viscosity (middle) and scalar radiation intensity (right) in the core cavity. All calculations were performed for 2 hours after shutdown at initial operating power of 60 MW.

The turbulent viscosity is shown in Figure 4 (middle). The value of viscosity is obviously larger than the laminar viscosity by several orders of magnitude, justifying the use of a high Reynolds number turbulence model.

Figure 4 (right) shows the scalar radiation intensity field. Several remarks should be made related to the applicability of the radiation model. Although the use of P_1 approximation is expected to be a good approximation in the bed region, the validity of the method breaks down in the cavity, where the concentration of the fuel particle is practically zero. The radiation intensity in the cavity was found to be strongly dependent on the volume fraction of the particles. When the particle volume fraction is low, the temperature of the inner reflector wall dictates the radiation equation, giving a small value of intensity. The result is a strong underestimate of the radiative transfer from the packed bed to the walls of the freeboard. When the particle volume fraction is larger, the temperature of the particle (or the gas) becomes dominant and gives a larger value of intensity. An improved method for treating the radiative transfer in the cavity is thus necessary. Therefore, the conclusion that the decay heat corresponding to powers above 55 MW cannot be removed entirely by passive means is uncertain.

5. Conclusions

Numerical simulations were performed to investigate the possibility of passive decay heat removal in a fluidized bed nuclear reactor. The maximum fuel temperature in the core increases in the first few hours after reactor shutdown and reaches a maximum value before decreasing slowly. For some values of the initial operating power, the maximum fuel temperature exceeds the recommended permissible limit, indicating that the decay heat cannot be removed via passive means. The presence of convection in the cavity and radiation in the particle bed is effective to transfer heat to the reflector whereas only conduction and radiation heat transfer are dominant in the particle bed. The radiation treatment was found to be questionable owing to the large mean free path in the cavity above the bed and should be replaced by a more elaborate model in the future.

References

1) Agung, D. Lathouwers, T.H.J.J van der Hagen, H. van Dam, C.C. Pain, C.R.E. de Oliveira, A.J.H. Goddard, M.D. Eaton, J.L.M.A. Gomes, B. Miles, "On a New Design of a Fluidized Bed Nuclear Reactor. Part I: Design Modifications and Steady State Features", to be submitted to Nucl. Techn.
2) J.L. Kloosterman, V.V. Golovko, H. van Dam, and T.H.J.J. van der Hagen, "Conceptual Design of a Fluidized Bed Nuclear Reactor", Nucl. Sci. Eng., **139**, 118 (2001).
3) International Atomic Energy Agency, "Fuel Performance and Fission Product Behaviour in Gas-Cooled Reactors", IAEA-TECDOC-978, Vienna (1997).
4) M. Kaviany, "Principles of Heat Transfer in Porous Media", Springer, New York (1991).
5) D. Lathouwers, J. Bellan, "Modeling of Dense Gas-Solid Reactive Mixtures Applied to Biomass Pyrolysis in a Fluidized Bed", Int. J. Multiphase Flow, **27**, 2155 (2001).
6) E.W. Lemmon, M.O. McLinden, D.G. Friend, "Thermophysical Properties of Fluid Systems" in NIST Chemistry WebBook, NIST Standard Reference Database Number 69, Eds. P.J. Linstrom and W.G. Mallard, National Institute of Standards and Technology, Gaithersburg MD, 20899, (2003)

7) J.K. Fink, “Thermophysical Properties of Uranium Dioxide”, J. Nucl. Mat., **279**, 1, (2000).
8) A.T. Dinsdale, “SGTE Data for Pure Elements”, CALPHAD, **15**, 317, 1991.
9) R. Siegel, J. R. Howell, “Thermal Radiation Heat Transfer”, Taylor and Francis, Washington (2001)
10) “Berechnung der Nachzerfallsleitung der Kernbrennstoffe von Hochtemperaturreaktoren mit Kügelförmigen Brennelementen”, Technical Report DIN 25 485 (1990).